Computational Uncertainty in CFD Associated with Spatial and Temporal Discretisation and Non-linear Methods Design

D. Drikakis, M. Hahn, A. Mosedale, E. Shapiro and B. Thornber[1]
Department of Aerospace Sciences
School of Engineering,
Cranfield University
Cranfield, Bedfordshire MK43 0AL, UK

d.drikakis@cranfield.ac.uk

ABSTRACT

Many flow fields of industrial interest require the accurate simulation of transition to turbulence from an initially laminar flow field, however, there exist a huge number of possible numerical methods one can employ for a given situation. This paper highlights the computational uncertainty associated with the choice of numerical method when simulating a turbulent flow field on under-resolved grids. As a motivating example, it is shown that for a swept wing at high Reynolds number Godunov-type methods gain very good results in the turbulent regions, but accuracy is limited in the transition region close to the leading edge. Two-dimensional instabilities are investigated to highlight in isolation the importance of defining in a physically relevant manner the resolving capability of the numerical scheme employed. An educated choice of numerical method can easily save one eighth of the computational expense, and a reduction in computational uncertainty associated with under-resolved flow features in both two and three dimensions. *Furthermore, simulations of a multimode shear instability demonstrate that even two closely related discretisation methods can produce significantly different behaviour during the transition regime, particularly if the initial perturbations are not well resolved on the given grid with the given numerical method.*

1.0 INTRODUCTION

The development of modern computational fluid dynamics methods encompasses a number of numerical components and modelling assumptions which can affect both accuracy and efficiency of incompressible and compressible flow simulations. In the simulation of industrial flows it is often necessary to capture several different stages in the development of a turbulent flow field. However, the linear, non-linear and fully turbulent stages in the growth of an initial perturbation often place contradictory requirements on the numerical methods used. For example, in a fully developed turbulent flow it is desirable that the numerical method provides some kind of damping to replace the action of subgrid stresses on the resolved motions. However, in the early linear and non-linear stages it is important to allow the perturbations to grow without excessive damping from the numerical method. Typically at the early stages these perturbations are severely under-resolved. This paper demonstrates that the choice of numerical scheme strongly influences the solution in time-dependent transitional flows, especially if the user does not consider carefully the capability of the numerical method employed.

The structure of this paper is as follows. Section 2 illustrates the problems associated with transitional flows in high-Reynolds number, Large Eddy Simulation (LES) of a swept wing configuration. The LES

[1] Authors are listed in alphabetical order

Drikakis, D.; Hahn, M.; Mosedale, A.; Shapiro, E.; Thornber, B. (2007) Computational Uncertainty in CFD Associated with Spatial and Temporal Discretisation and Non-linear Methods Design. In *Computational Uncertainty in Military Vehicle Design* (pp. 41-1 – 41-18). Meeting Proceedings RTO-MP-AVT-147, Paper 41. Neuilly-sur-Seine, France: RTO. Available from: http://www.rto.nato.int.

strategy employed throughout the paper is based on high-resolution and very high-order methods (up to ninth-order), which act as an implicit subgrid scale model due to their non-linear dissipative properties; this approach is also known as implicit LES (ILES). These simulations show that although the computational results are in very good with the experiment in the regions of fully developed turbulent flow, including the near-wall flow, discrepancies between experiment and simulation occur at the leading edge due to the highly under-resolved grid in this area. These effects are investigated in isolation in Section 3, detailing the various mechanisms which influence the early stages of growth of a shear-induced instability, and a shock-induced instability. Uncertainties in the computation due to the resolution of the numerical scheme (second- to ninth-order), Mach number effects and initialisation of the flow field are discussed. Section 4 extends the understanding gained from the single mode simulations to more complex simulations of transition to turbulence through a multimode shear instability, and the transition of regular vortices to a fully turbulent flow in the Taylor-Green problem. Finally, Section 5 draws conclusions on the performance of high-resolution methods.

2.0 HIGH REYNOLDS FLOW OVER A SWEPT WING

A motivating example for investigating the behaviour of different numerical methods in transitional flows is a simulation of a swept wing at a Reynolds number of approximately 210,000, based on the free-stream velocity and root chord length, and a near incompressible Mach number of 0.3. The flow around the swept wing geometry has been computed using a third-order accurate MUSCL scheme in space and a third-order accurate Runge-Kutta method in time [8]. For the numerical discretisation, a C-O-type grid comprising a total of 12.7M points has been employed. It features z^+ values ranging from 1 in areas of separated flow to 5 at the leading edge and the computational domain measures 6c, 6.14c and 5c (c is the root chord length) in x, y and z directions, respectively.

The general flow topology is illustrated in Figure 1 by instantaneous streamlines, slices of iso-vorticity contours and pressure coefficient distribution on the suction side of the wing. Similar to sharp-edged delta wings, the shear-layer emanating from the leading edges rolls up into a distinctive leading edge vortex system which breaks down as it progresses towards the trailing edge. After breakdown, a non-symmetrical turbulent flow-field develops over the outer section of the wing.

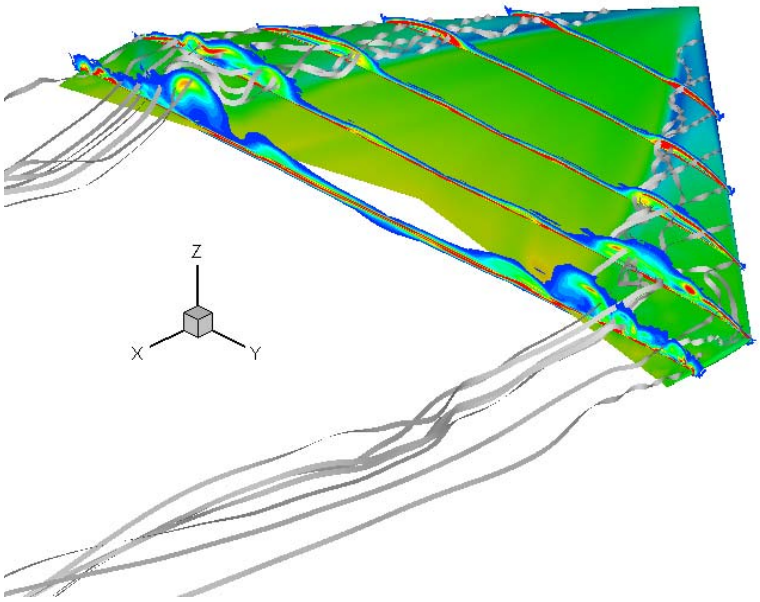

Figure 1: Instantaneous streamlines, slices of iso-vorticity contours and pressure coefficient distribution on the suction side of the wing.

A quantitative comparison between the simulation, labelled as "CNS3D", and experimental 3D-LDA measurements [22] has been performed for the averaged streamwise velocity component as well as for the normal and shear stress components, see Figure 2. Three chord-wise positions (10%, 50% and 90% local chord) at a spanwise location of 90% half-span (outboard of vortex breakdown) are presented here and all data has been normalised by the free-stream velocity and the root chord length. In the fully separated flow region near the wing tip, the velocity profiles from the simulation and the experiment presented in Figures 2(a) to 2(c) match at all chord-wise positions. Regarding the Reynolds stresses away from the under-resolved area near the leading edge, the shear stresses compare closely with the experimental data in shape and magnitude, see Figures 2(e) and 2(f). However, the differences in Figure 2(d) regarding the magnitude of the Reynolds stresses closer to the leading edge hint at the inadequate grid resolution in the regions of highly accelerated flow.

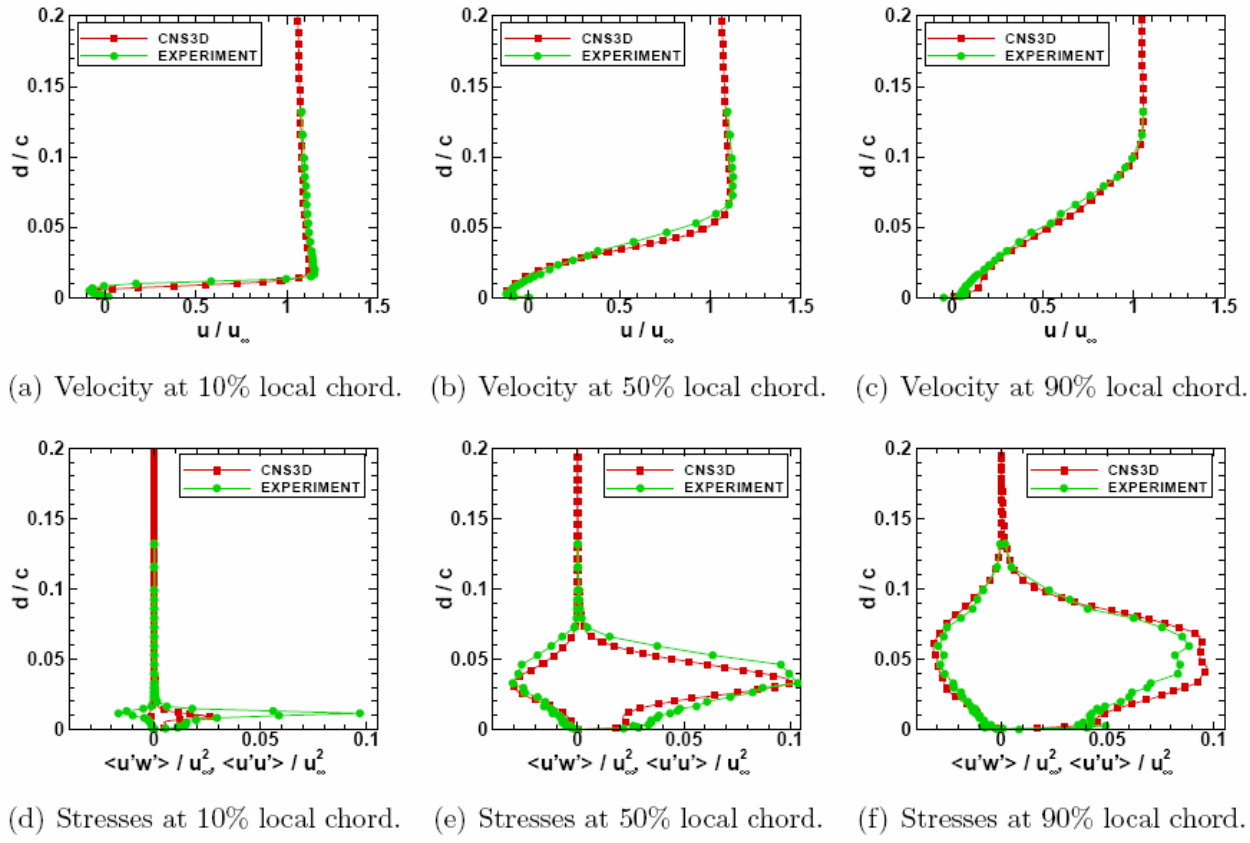

(a) Velocity at 10% local chord. (b) Velocity at 50% local chord. (c) Velocity at 90% local chord.

(d) Stresses at 10% local chord. (e) Stresses at 50% local chord. (f) Stresses at 90% local chord.

Figure 2: Comparison between averaged velocity profiles and stresses from experiment and results obtained with ILES for different locations along the local chord at 90% half-span.

Although the mean velocities obtained in the simulation are very accurate, the representation of the fluctuating components lacks confidence near the leading edge. Here, prediction of the transitional flow instabilities emanating from the separation region is of paramount importance, especially since they are almost always highly under-resolved in practical applications. This example shows that numerical investigations of fundamental instabilities are not only of academic interest, they also have a great impact on most engineering problems, e.g. the prediction of fluid structure interactions leading to flutter and fatigue.

3.0 GROWTH OF A SINGLE INSTABILITY

3.1 Shear Instability

One of the most common instabilities is the shear, or Kelvin-Helmholtz instability [10]. This occurs when there is a gradient in flow velocity, such as in boundary layers, or two flows joining behind a flat plate. Given a small perturbation in the flow, the mixing layer grows in time. The test case considered in this section is a single mode Kelvin-Helmholtz instability. The computational domain is initialised with y-direction velocities V on the right hand side, and −V on the left hand side of a square domain. An initial perturbation of magnitude 0.1V is applied to the interface to seed the single mode instability [21]. The development of this instability using a grid of 32× 32 is shown in Figure 3, by tracking a passive scalar which is initialised as 1 in the right hand flow, and 0 in the left hand flow.

This section will investigate two commonly known, but often forgotten sources of error. The first is the effective resolution of a given numerical scheme. It has become common to measure the effective resolution of a numerical scheme via the 'order of accuracy', however this measurement does not give a direct indication of the resolving power of the numerical method. For example, it is not clear if a second-order scheme requires ten cells to accurately resolve a vortex, or thirty. Once this criterion is measured, it represents the minimum size of eddy which is accurately represented in the full scale simulation (i.e. close to the leading edge in the swept wing). It is, of course, a closely related function of the resolution of the numerical method chosen. The second phenomenon investigated is the influence of Mach number on the solution gained for a compressible numerical scheme. It is well known that the solution gained using compressible (Godunov-type) methods degrades at low Mach [19]. This is illustrated clearly by varying the Mach number of the single mode perturbation.

Figure 3 compares the performance of two standard second order methods [18, 17] when resolving the growth of the single mode perturbation at Mach=0.2. At 32^2 resolution the perturbation is clearly well resolved and the characteristic Kelvin-Helmholtz roll-up of the vortex is visible. However, reducing the grid size to 16^2 shows that both of the second-order methods fail to reproduce the eddy structure at 32^2, indeed the Minbee-based limiter solution does not produce a vortex at all. Clearly, the second-order methods require greater than 16 cells per vortex to resolve the growth accurately. This is not a new result, however in modern turbulence simulations it has become commonplace to require that a Kolmogorov spectrum is resolved all the way to the cut-off frequency. It is unrealistic to expect a numerical scheme to resolve perfectly a vortex in just 2 cells, and an excellent result for very high-order methods would be accurate resolution of vortices which span 8 cells. Any kinetic energy in vortices smaller than this is either numerical noise, or damped by numerical dissipation.

Figure 4 shows the performance of a fifth-order MUSCL (M5) [11] and ninth-order WENO (W9) [1] methods applied to the same single mode problem at 16^2 cross-section. The results are significantly improved upon those for the second-order limiters, and even factoring in the extra computational time (≈ 20% for M5 and ≈ 350% for W9) they are computationally more effective. Note that at a resolution of 8 × 8 the very high order methods also fail to capture the development of the vortex. Considering that around the leading edge of the swept wing there are approximately 8 cells in the transitional zone it is not surprising that the growth of the small perturbations are not captured accurately.

Moving onto the behaviour of Godunov-type methods at low Mach numbers, Figure 5 shows the development of the Kelvin-Helmholtz instability at Mach=0.02 with the fifth-order method. As can be seen there is a slight perturbation of the shear layer, but further development is prevented due to the dissipation of the numerical scheme. It has been shown that the dissipation of kinetic energy in a numerical scheme increases as 1/Mach [15]. Thus there is a ten-fold increase in dissipation by moving from Mach=0.2 to Mach=0.02. At this Mach number there are two options - either switch to an incompressible code (or a non-shock capturing/perturbation model), or implement a correction which

gradually central differences the velocity components as Mach tends to zero [16]. Results using this method in conjunction with fifth-order MUSCL are also presented in Figure 5 (labelled 'M5+LM') demonstrating greatly improved resolution of the vortex.

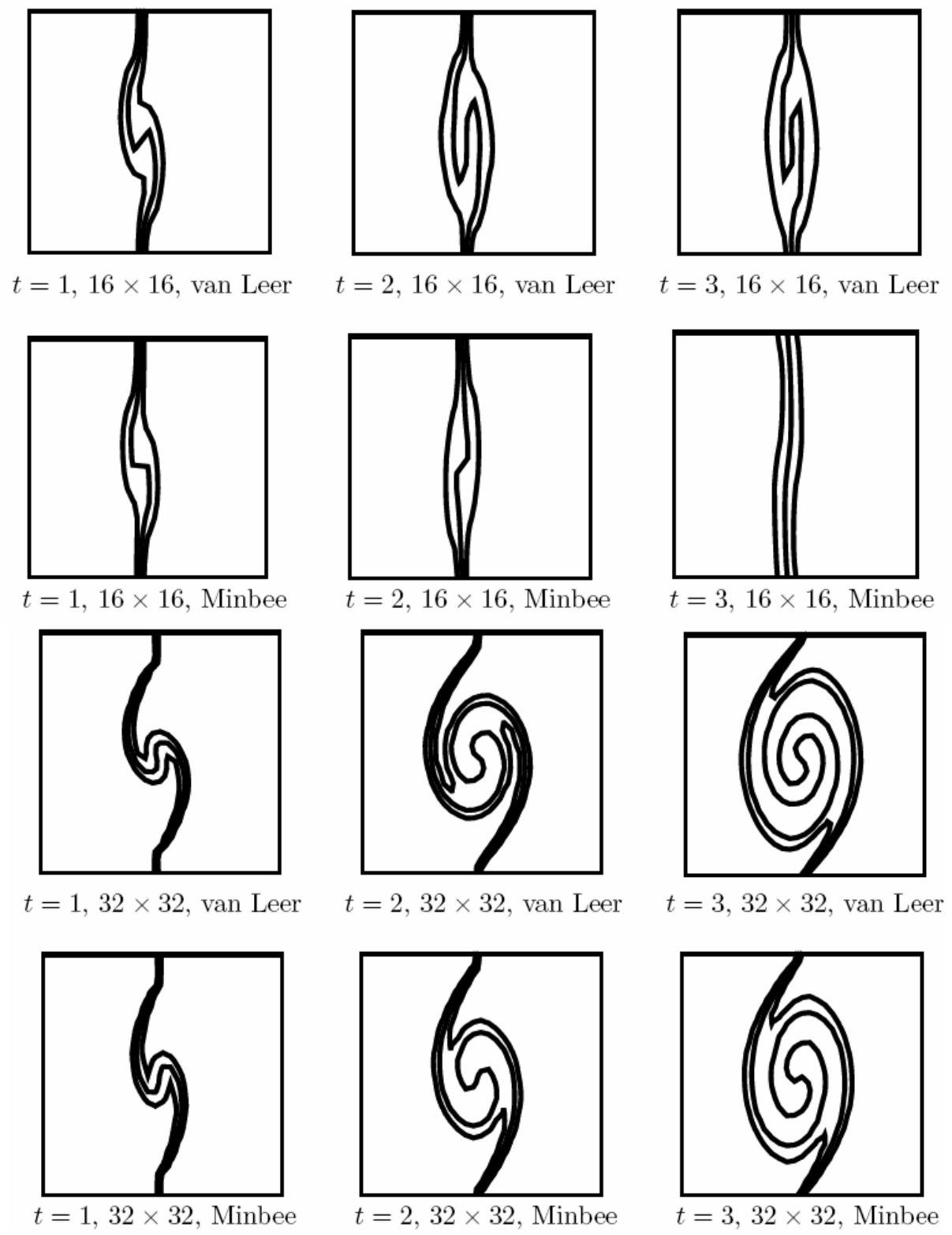

Figure 3: Contours of volume fraction (0.25, 0.5, and 0.75) of the passive scalar for the Kelvin-Helmholtz instability using two different second-order methods

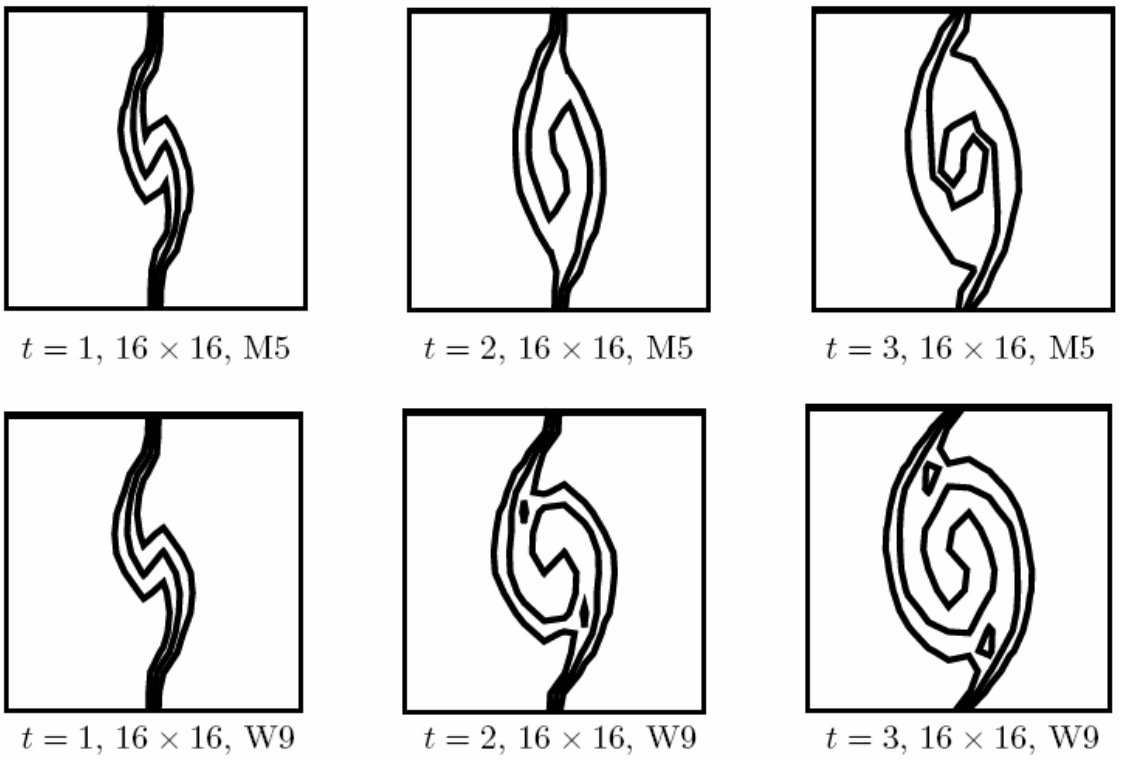

Figure 4: Contours of volume fraction (0.25, 0.5, and 0.75) of the passive scalar for the Kelvin-Helmholtz instability using very high-order methods

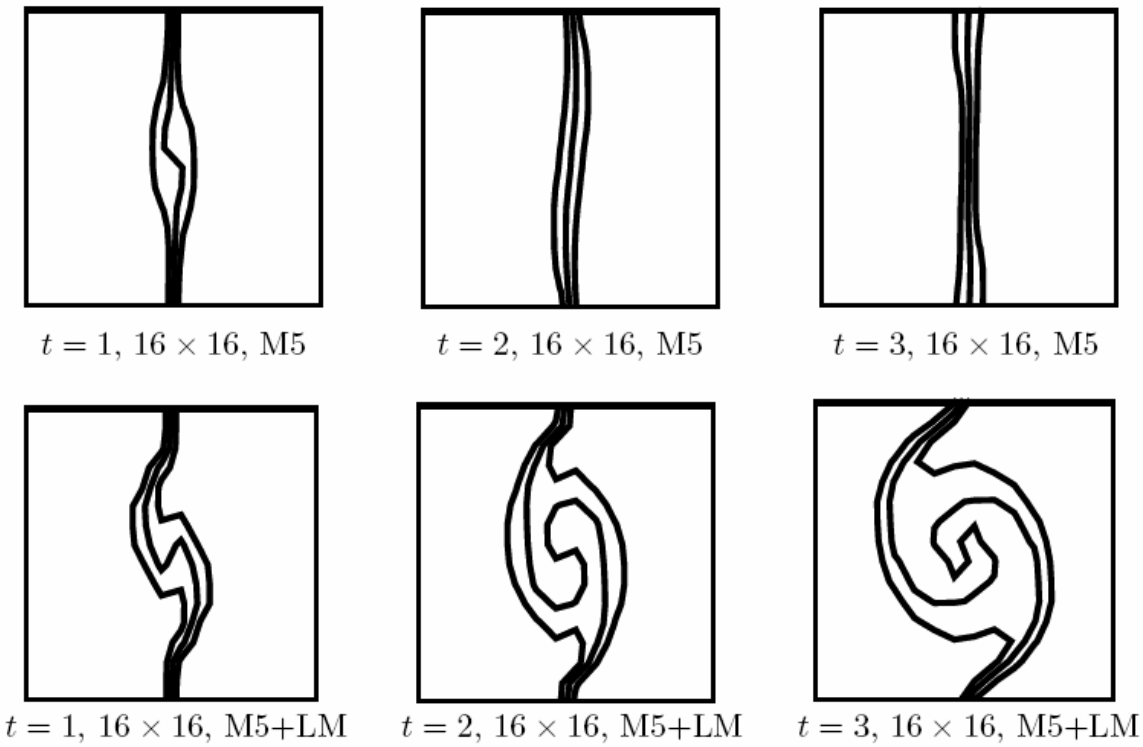

Figure 5: Contours of volume fraction (0.25, 0.5, and 0.75) of the passive scalar for the Kelvin-Helmholtz instability at three different times at Mach=0.02

In summary, care must be taken to define the 'operating limits' of the numerical scheme with respect to resolution of vortex features and the Mach number of the system of interest, as the common custom of labelling numerical schemes by their order of accuracy is not the sole important measure in the specification of numerical grids, or choice of numerical methods in practical simulations.

3.2 Shock-Induced instability

The Richtmyer-Meshkov Instability (RMI) is caused by a shockwave passing through a perturbed gas interface. As such, it requires accurate treatment of shock waves, turbulence and multiple gases. Three-dimensional multiple mode problems are very challenging problems to simulate or produce in experiment. It is useful to look at the two-dimensional single mode case to compare schemes though two-dimensional stability still does not guarantee a sensible solution of the three-dimensional problem. In order to gain some validation for the numerical method, a simulation based on the experimental work of Jacobs [9] was set up. This experiment used a new approach to create the material interface to remove the effects of membranes that had always affected previous experimental work. The interface was a single-mode sinusoid between air and SF6, and in the case studied the incident shock was of strength 1.3.

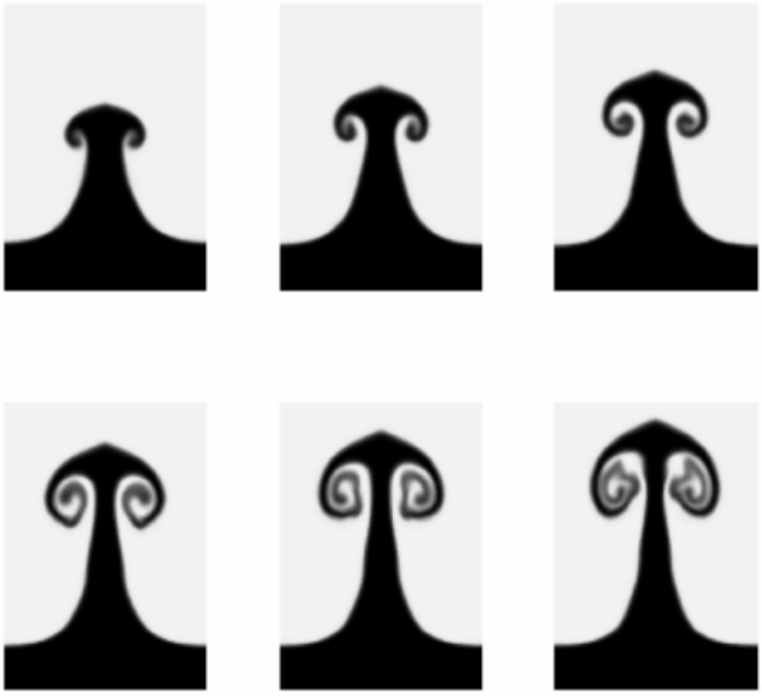

Figure 6: Plot of volume fraction of SF6 showing the development of the instability over time, using 5th-order WENO on 80x240 grid, based on a sharp initial interface

The simulation was first initialised as perfect - pure gases on either side of the interface with a pre-shock Atwood number of 0.692 - whereas due to necessity in creating the perturbation the experiment has some diffusion leaving some air mixed with the SF6. The experimental and numerical problems are similar enough to bear comparison, not only in the visual appearance of the instability but also the growth rates of the bubble and spike, which are appropriately non-dimensionalised.

The typical growth of the instability is shown in Figure 6 for a reasonably well resolved scheme, where the dark region represents the SF6 in a plot of volume fraction. After the initial linear growth phase the vorticity deposited by the shock wave can be seen to be gathering at the head of the instability as it starts to pull material round the sides. This roll-up continues, establishing clear vortical structures, which then start to manifest the secondary instability seen in experiments as a series of small Kelvin-Helmoholtz features which disturb the smooth lines of the vortex leading to an eventual breakdown into turbulence.

Comparison with experiment will quickly reveal however that the curvature of the mushroom head is flawed in this simulation. This is due to how the initial perturbation is resolved on the Cartesian grid, indeed it was found there are many factors to consider in setting the initial conditions as these high-order schemes are very sensitive to small differences.

While the vortex dynamics dominate the flow and can destabilise the upper surface, there is no evidence that the shape of the very tip of the instability has any major impact on the formation of neither the vortices nor the breakdown to turbulence. The comparison of methods conducted by Liska and Wendroff [12] in which they consider the Rayleigh-Taylor instability, which is closely related to Richtmyer-Meshkov, shows a host of unphysical and unpredictable features at the head of the instability depending on the method used. This is a manifestation of how different methods respond to "errors" in different ways. Should the initial conditions be perfectly specified as part of a continuum then one would expect a properly rounded tip to the instability but this is one area that demands very careful approximations to be simulated accurately.

Figure 7 shows the comparison of different order of accuracy methods over a range of coarse grids with 20, 40 or 80 cells per wavelength. At the coarsest resolution very little can be seen, though it is well worth noting that the overall amplitude of the instability at this time is comparable with the more highly resolved simulations. With less than 20 cells this soon ceases to be the case, so this point can be considered to be when the primary instability is resolved. It is hard to see much difference between the schemes, however the 9^{th}-order WENO method gives an indication that some genuine vorticity is at work at the top of the spike causing the shear layer to roll up. At 40 cells across, features are much more clearly visible. The 9th-order WENO interpolation shows clear vortical roll-up at this stage and the mushroom shape compares favourably to the experimental results. The most resolved picture as obtained by the 9^{th}-order WENO method has already passed the secondary instability within the vortex coil and has broken down into a turbulent mixed area. Also quite clearly seen is some separated fluid drawn down from the vortices, which is caused by small Kelvin-Helmholtz instabilities that form on the stem. At this resolution only the effects of distortion can be seen. They are not found in the experiment due to the slightly diffuse nature of the initial perturbation. By contrast these simulations had a sharp discontinuity (to the level of resolution of the grid) and the higher-order schemes do not carry sufficient dissipation to damp out the numerical errors.

As mentioned before, the growth rates seen in all the simulations are very similar. Figure 8 shows the non-dimensionalised plot of amplitude over time. The symbols represent the experimental measurements taken from Jacobs' paper and the lines show the results of the simulations for all resolutions and schemes. It is expected that if the simulations were extended to much later time there would be increasing deviation as the non-linearity of the growth becomes dominated by the turbulent mixing - a phenomenon not captured at the lower-resolutions. However, it is clear that the schemes can capture the main non-linear growth region, which the theoretical models struggle to predict, and having validated the method against these experiments a parametric study could relatively swiftly be carried out to improve the theory of this growth via the simulations.

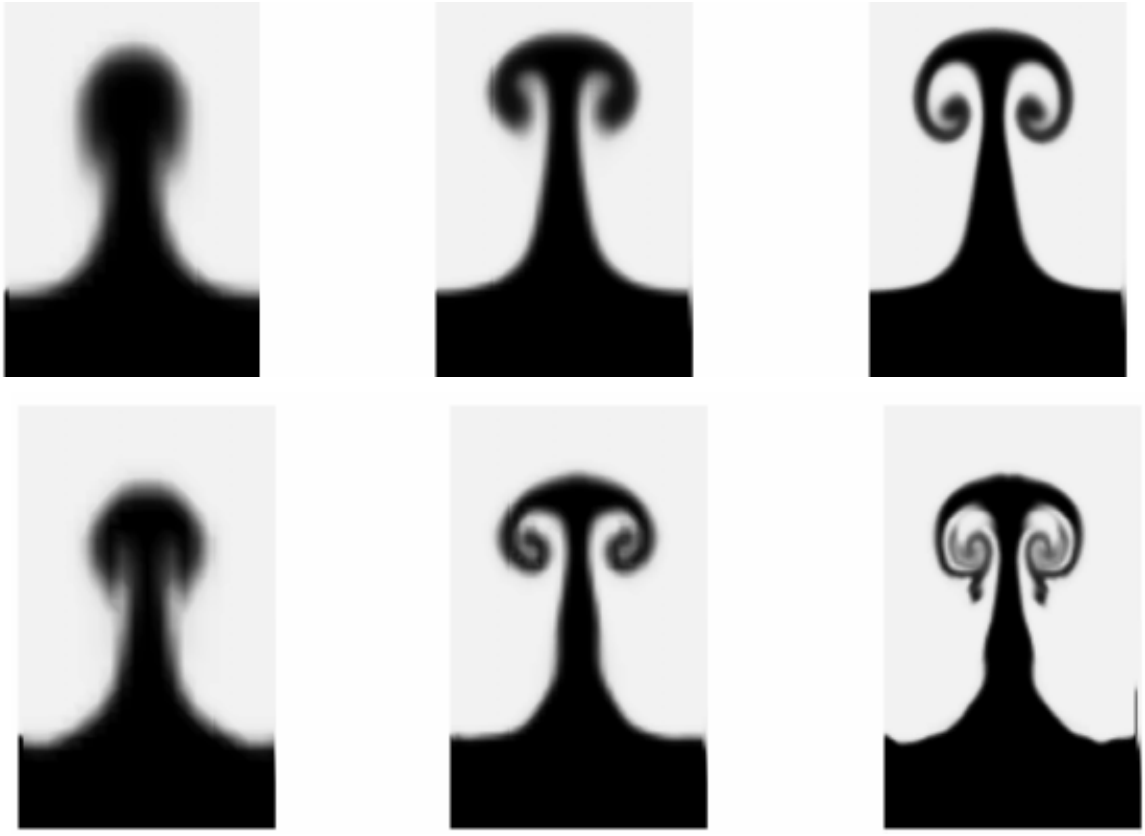

Figure 7: Volume fraction plots of Richtmyer-Meshkov Simulations with 20, 40 and 80 cells per wavelength (columns 1 to 3, respectively) and reconstruction method, Van Leer 2nd-order (upper row) and 9th-order WENO (lower row), for sharp initial interface and Atwood No. of 0.692

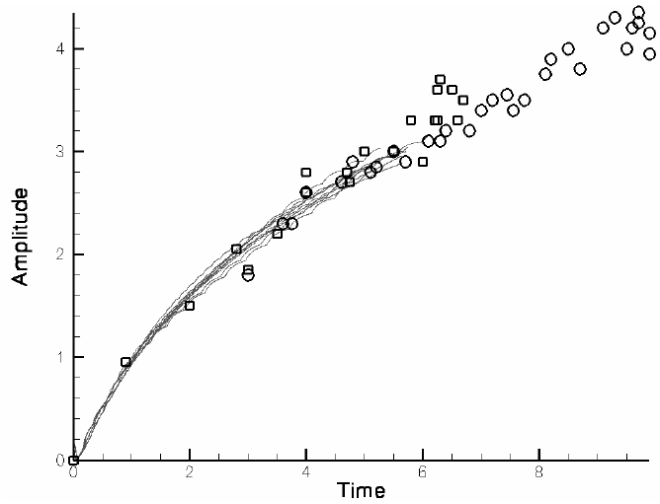

Figure 8: Growth of instability, as predicted by different methods (lines), compared to experimental measurements (circles relate to equivalent problem, triangles to a weaker shock case), non-dimensionalised

The 9th-order WENO method is more expensive than the 2nd-order van Leer by a factor 3, but is better value for the level of fine-scale detail it provides. More refined grids and further comparison with experimental results is required to assess whether such detail is physically correct, however it has been noticed that the higher-order schemes are particularly sensitive to very small differences in initial conditions and there is a limit to how well the experiment can be modelled to achieve highly comparable results with simulations. Indeed, it may not be possible with this problem to identify whether the scheme is introducing spurious errors or merely reflecting discrepancies in other parts of the model. Thus far the behaviour has appeared physical, and with coarse simulations the WENO methods do well at mimicking the results of the second-order schemes on finer grids, but it has not been definitively seen that both approaches converge to the same solution for this problem.

One of the critical issues of very high-order methods is that the numerical scheme becomes increasingly sensitive to the initial conditions. As has been highlighted within this section, WENO methods allow the use of smaller grids. However, when a smaller grid is used, the initial conditions, or indeed any complex geometry in the domain (e.g. a wing) are not represented as accurately.

The first important modelling assumption used in the previous examples was that the initial interface was sharp, however in experiments it was diffuse. To investigate the effect of the initial condition, the transition between the two gases was spread linearly over 5mm, and the grid resolution increased to 400 cells, using fifth-order MUSCL. The results are shown in Figure 9. The sharp interface suffers from spurious Kelvin-Helmholtz vortices along the neck of the instability, which are not present in the experiment. This is due to the absolute instability of the sharp discontinuity. The diffuse interface significantly reduced the unwanted instabilities - although it did not suppress them entirely for the higher resolution runs.

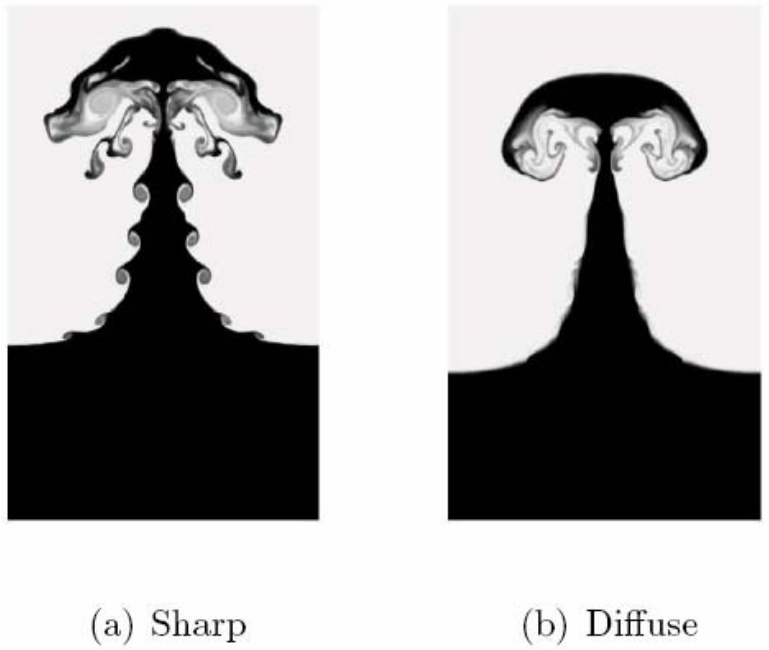

Figure 9: Comparison of sharp and diffuse initial interfaces for 5th-order MUSCL scheme on 400 cell cross-section

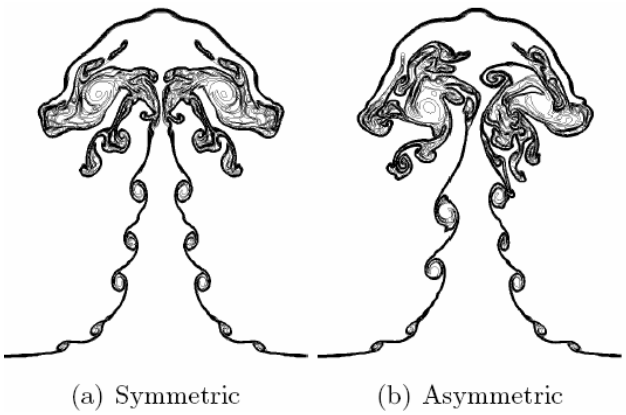

Figure 10: Comparison of alignment of initial condition for 5th-order MUSCL scheme on 400 cell cross-section

A further important point to note is sensitivity of the final solution (especially in two dimensional simulations) to the position of the initial condition with respect to the grid. To measure the above two simulations were run, the first is perfectly centred, i.e. the single wave is exactly centred on the grid. The second initialisation shifts the wave by 10^{-6}% with respect to the grid centre. Figure 10 compares the two initialisations. This illustrates that the 'errors' are coming from the initial conditions rather than the solution method, and care must be taken to ensure that grid effects are not dominating the solution in flows which are expected to be symmetric.

Figure 11 shows the fifth-order WENO result for 400 grid cells using this diffuse interface, as well as how it compares overlayed on the 80 cell image. The overall amplitude is comparable as expected, as is the general bubble shape and position of the vortices. Although the coarser simulation does not evidence the secondary instability that leads to breakdown of the vortices, it is up to this point a very good approximation of the flow. This compares very well with the experimental images. However as has been noted the simulation is highly sensitive to initial conditions and more highly-resolved simulations indicate that the initialisation is not perfect and is more a happy coincidence that overly dissipative simulations of an unstable initial condition results in a plausible looking flow. The issues investigated in this test case however are not expected to affect better posed problems for which the initial condition is well defined and allows for a degree of uncertainty.

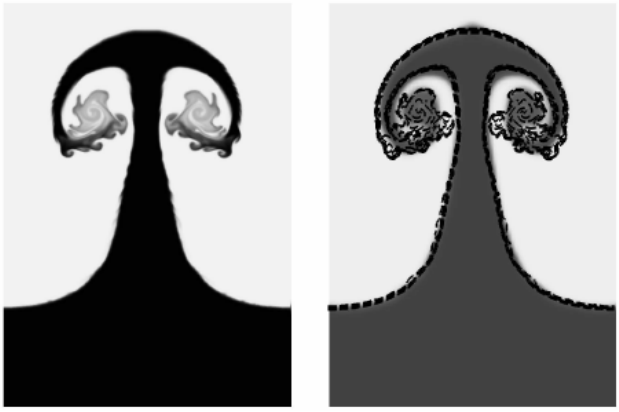

Figure 11: Fine grid (400 cell) 5th-order WENO simulation compared to coarse 80 cell simulation

4.0 TRANSITION TO TURBULENCE

4.1 Taylor-Green Vortex

The Taylor-Green Vortex is a fundamental case that has been used as a prototype for vortex stretching and the consequent production of small-scale eddies in the context of transition to turbulence [3]. Here, the performance of various numerical schemes for the discretisation in time and space are investigated with regard to the dynamics of the evolving vortex field. The configuration involves triply periodic boundary conditions enforced on a cubic domain of length 2π using 64^3 and 128^3 computational cells. Furthermore, the flow field was initialised with a single mode velocity field and the initial pressure is given by the corresponding solution of a Poisson equation [5].

In order to assess the behaviour of different numerical methods [6], the evolution of the volumetric enstrophy in time is shown in Figure 12. First, the effect of various Runge-Kutta time-stepping methods has been investigated. Here, all simulations have been performed on a grid comprising 64^3 points and employing a third-order accurate MUSCL scheme. The resulting enstrophy displayed in Figure 12(a) is virtually identical for a second-order method (RK2), a second-order TVD method (RK2TVD), a third-order TVD method (RK3TVD) and an extended stability method (RK3HI) for up to twenty eddy-turnover times. This is expected as the CFL condition restricts the maximum time step size to the cell size divided by the speed of sound.

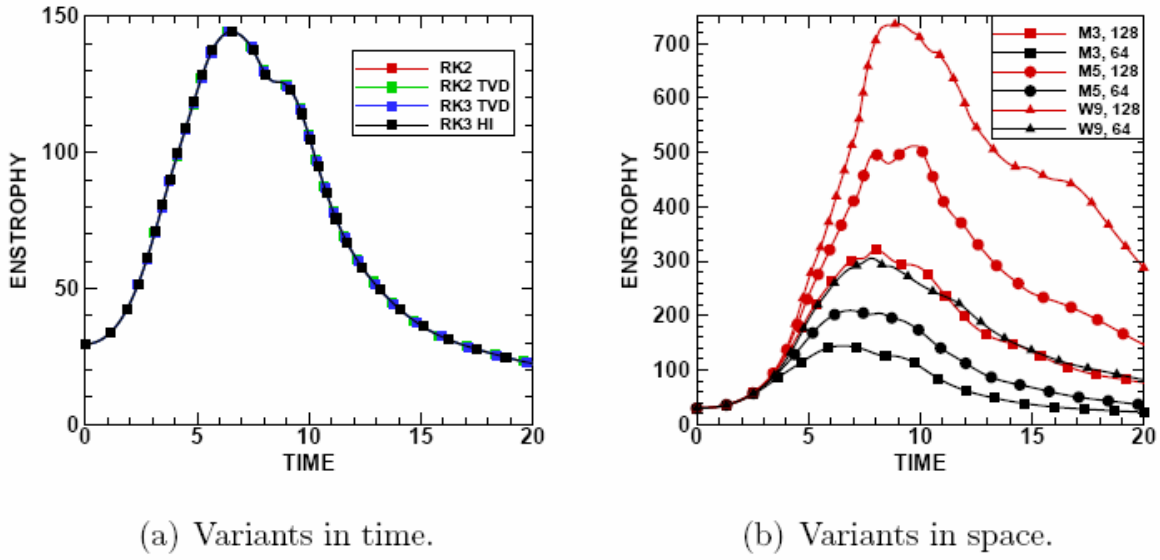

Figure 12: The effect of different discretisation techniques on the evolution of enstrophy.

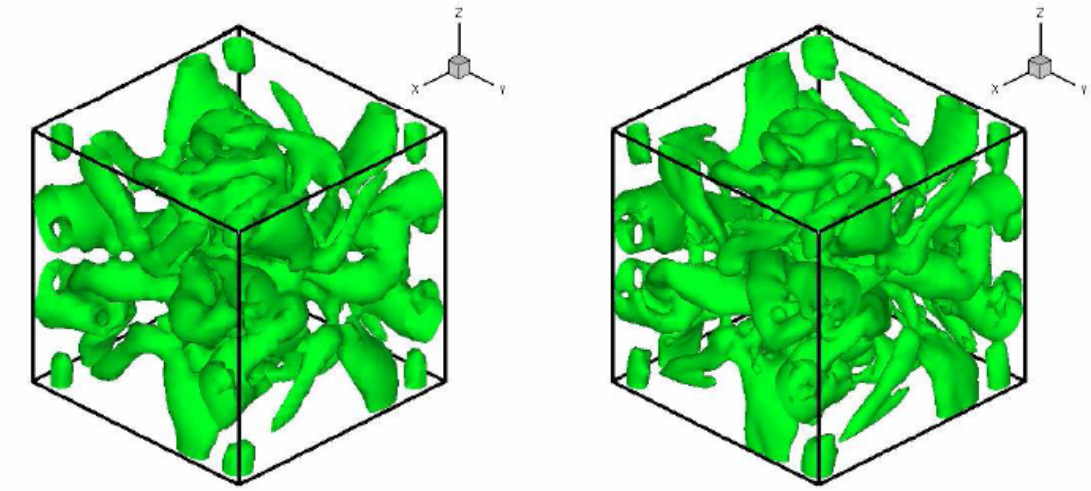

(a) W9 on 64^3 computational cells. (b) M3 on 128^3 computational cells.

Figure 13: Iso-surfaces of the Q-criteria near the peak in enstrophy at time t = 9.

While the specifics of the time integration method seem to have a negligible impact on the evolution of the vortex field, the same cannot be said for the choice of the spatial discretisation scheme. Evidence for this statement is revealed in Figure 12(b) showing the evolution of enstrophy as predicted on two grid sizes (64^3 and 128^3) by three different numerical methods: a third-order accurate MUSCL scheme (M3), a fifth-order accurate MUSCL scheme (M5) and a ninth-order accurate WENO scheme (W9). Although the peak in enstrophy appears at roughly the same time for all the methods, the magnitude differs substantially. This leads to the conclusion that the dynamics dictating the transition from the large-scale dominated initial state to a flow field featuring increasingly smaller vortex filaments is captured more accurately on the lower resolution by the higher-order methods. Note the remarkable similarity between the simulations using the third-order MUSCL scheme on 128^3 computational cells (M3 128) and the ninth-order WENO scheme on 64^3 computational cells (W9 64). This impression is confirmed by considering the vortex structure during the peak in enstrophy as visualised in Figure 13 according to the Q-criteria (only one-eighth of the total cube shown here). As expected, the flow predicted by the W9 scheme exhibits very similar structures compared to the results from the M3 scheme obtained at twice the resolution in each spatial direction. This is consistent with the observations noted with respect to the single mode instabilities, demonstrating that results gained using prototype flows in Section 3 readily extend to three dimensional flows.

4.2 Multimode Kelvin-Helmholtz

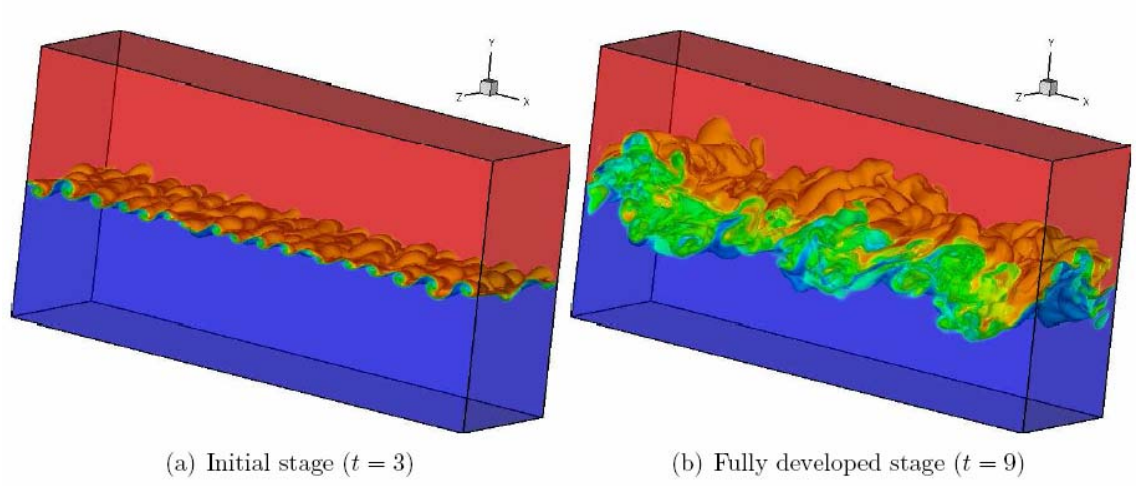

Figure 14: Transition to turbulence in the mixing layer

Results obtained through the investigation of single-mode behaviour in Kelvin-Helmholtz instability are readily applicable to much more complicated transitional flows. Fully developed turbulent flows tend to loose memory of the initial condition and the effect of the under-resolved scales of the flow on the large scales tends to stabilise. On the other hand transitional and absolutely unstable flows introduce additional uncertainties into turbulent flow simulation associated with the initial conditions and the effect of under-resolved modes onto the solution. Inviscid Kelvin-Helmholtz instability is a classical example of an absolutely unstable problem for which the growth rate of the perturbation is proportional to e^k, where k is the wave number [4]. Since the short waves grow much faster than the long waves, transition is determined by the resolution of the numerical scheme and the dispersive properties of the numerical scheme, which are responsible for the excitation of the modes which were not in the initial perturbation spectrum.

Figure 14 shows the evolution of the mixing layer in a 4x2x1 domain. The ILES computations were performed on grids ranging from 257 × 129 × 65 to 513× 257 × 129 points using a characteristic-based scheme [7] and second-order MUSCL reconstruction with various limiters - Van Albada, Van Leer and SuperBee (see, for example [17]). The mixing layer development starts with the initial linearly unstable stage, characterised by the exponential growth, and undergoes transition to turbulent regime characterised by the linear growth of the mixing layer thickness. Figures 14(a) and (b) show iso-surfaces of the passive scalar at the initial stage of the mixing layer development and fully turbulent stage, respectively.

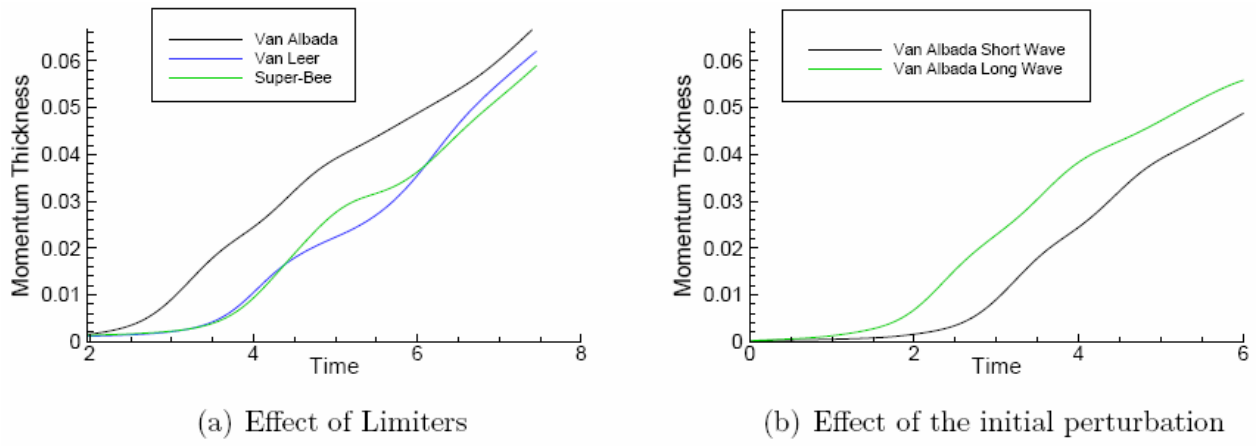

Figure 15: Mixing layer growth

The behaviour of the fully developed turbulent stage can be characterised by the development of momentum thickness. In order to demonstrate the uncertainty associated with the initial condition and under-resolved wave-lengths in the initial condition, an initial random divergence-free perturbation, with the spectrum specified according to [20] and either short-wave perturbation with wave lengths ranging from $4\Delta x$ to $8\Delta x$ or long-wave perturbations with wave lengths ranging from $4\Delta x$ to $32\Delta x$, was considered. The standard deviation of $0.08\Delta x$ was used in both cases.

In the first case the perturbation is given in the wave-lengths, which are not resolved by the second-order scheme according to single-mode tests detailed in Section 3. The unresolved perturbation then dissipates while at the same time exciting long waves, which are resolved by the scheme. This process defines the transition point - once the long-waves which are resolved by the scheme become excited, the growth of the mixing layer starts and transition to turbulence occurs. Different second-order schemes with similar dissipation lead to different prediction of transition to turbulence. Figure 15(a) shows momentum thickness obtained with different limiters. In the fully turbulent stage similar growth rates are obtained, however the van Albada limiter leads to a faster transition. Figure 15(b) shows momentum thickness obtained with the same limiter and different initial perturbation. Exciting resolved wave-lengths results in faster transition to turbulence.

In self-similar mode, the momentum thickness grows linearly with time. Experimental studies of mixing layers yield growth rates of ≈0.016 (see, for example, [2]). DNS of temporal mixing layer by [14] yields the growth rate of 0.014. Current ILES computations yield growth rates of 0.011 to 0.013 for coarse and fine grid respectively. The results indicate that for the transitional flows, the initial conditions represent an important source of computational uncertainty and the application of schemes with same nominal order of accuracy can result in different predictions where transition to turbulence is concerned. Similar strong effects of a small change in initial conditions on the developing stage of the mixing layer have been observed experimentally [13].

5.0 CONCLUSIONS

Implicit Large Eddy Simulations of a swept wing configuration demonstrate very good agreement with experimental measurements at all stations. As is typical with such under-resolved flows, the agreement of Reynolds stresses with experiment is worse where transition occurs at the leading edge.

Simulations of single mode instabilities highlight key factors in quantifying the resolution of a numerical method. It is shown that typical second- and third-order Godunov-type methods require between 16-32

cells to resolve a single vortex. At the leading edge of the swept wing, there are only about 8 cells in the entire transition region. Next, it is demonstrated that below Mach=0.2 the dissipation of the numerical scheme severely damps the growth of instabilities, and the numerical method must be modified to gain accurate results. It is also shown that the resolving power of the ninth-order WENO is equivalent to the third-order methods with twice the points in each direction. It is clearly computationally more efficient.

The results carry over to fully three-dimensional simulations of flows in turbulent transition. The Taylor-Green vortex case demonstrates that the time stepping method is not a critical factor influencing the result of the numerical simulation. As demonstrated with the Richtmyer-Meshkov instability, the ninth-order WENO is significantly more accurate than the third-order methods, and importantly show the same flow structures at the same time on grids one eighth the size.

Finally, the multi-mode Kelvin-Helmholtz study shows that scheme resolution and dispersive properties are of particular importance when the transition to turbulence is considered. The transition is governed by the development of the initial perturbation and when this includes under-resolved modes, the initial growth rates are highly dependent on numerical method. In this case even two closely related methods (such as van Albada and van Leer, for example) can produce significantly different growth in the early stages of the instability, leading to different predictions of turbulent transition.

ACKNOWLEDGEMENTS

The authors would like to acknowledge financial support from EPSRC, MoD and AWE through the contracts EP/C515153-JGS (No. 971) and from EPSRC and the MSSTAR Defence Aerospace Research Partnership (MoD, DTI, BAE SYSTEMS, Rolls-Royce and QinetiQ) through the contract GR/S27436/01.
.

6.0 REFERENCE

[1] D.S. Balsara and C.-W. Shu. Monotonicity preserving weighted essentially nonoscillatory schemes with increasingly high order of accuracy. J. Comput. Phys., 160:405–452, 2000.

[2] J. H. Bell and R. D. Mehta. Development of a two-stream mixing layer from tripped and untripped boundary layers. AIAA J., 28:2034, 1990.

[3] M. E. Brachet, D. I. Meiron, S. A. Orszag, Nickel B. G., R. H. Morf, and U. Frisch. Small-scale structure of the Taylor-Green vortex. Journal of Fluid Mechanics, 130:411–452, 1983.

[4] P.G. Drazin and W.H. Reid. Hydrodynamic Stability. Cambridge University Press, 2004.

[5] D. Drikakis, C. Fureby, F. Grinstein, and D. Youngs. Simulation of transition and turbulence decay in the Taylor-Green vortex. J. Turbulence., 8(1):1–12, 2007.

[6] D. Drikakis and W. Rider. *High-Resolution Methods for Incompressible and Low-Speed Flows*. Springer Verlag, 2004.

[7] A. Eberle. Characteristic flux averaging approach to the solution of Euler's equations. Technical report, VKI Lecture Series, 1987.

[8] M. Hahn and D. Drikakis. Implicit Large-Eddy Simulation for Swept Wing Flow using High-Resolution Methods. AIAA-2008-0669, 2008.

[9] J. W. Jacobs and V. V. Krivets. Experiments on the late-time development of singlemode richtmyer-meshkov instability. Physics of Fluids, 17:034105, 2005.

[10] R.M. Kelvin. Hydrokinetic solutions and observations. Phil. Mag., 42:362–377, 1871.

[11] K.H. Kim and C. Kim. Accurate, efficient and monotonic numerical methods for multi-dimensional compressible flows part II: Multi-dimensional limiting process. J. Comput. Phys., 208:570–615, 2005.

[12] R. Liska and B. Wendroff. Comparison of several difference schemes on 1d and 2d test problems for the Euler equations. SIAM J. Sci. Comput., 25(3):995–1017, 2003.

[13] M. W. Plesniak, J. H. Bell, and R. D. Mehta. Effects of small changes in initial conditions on mixing layer three-dimensionality. Experiments in Fluids, 14(2):286– 288, 1993.

[14] M. M. Rogers and M. M. Moser. Direct simulation of a self-similar turbulent mixing layer. Phys. Fluids, 6:903–923, 1994.

[15] B. Thornber, D. Drikakis, and R. Williams. The dissipation of kinetic energy within Godunov schemes I: Theoretical analysis. submitted to J. Comput. Phys., 2007.

[16] B. Thornber, A. Mosedale, D. Drikakis, and D. Youngs. The dissipation of kinetic energy within Godunov schemes II: Numerical modification. submitted to J. Comput. Phys., 2007.

[17] E.F. Toro. Riemann Solvers and Numerical Methods for Fluid Dynamics. Springer-Verlag, 1997.

[18] B. van Leer. Towards the ultimate conservative difference scheme.IV. a new approach to numerical convection. J. Comput. Phys., 23:276–299, 1977.

[19] G. Volpe. Performance of compressible flow codes at low Mach number. AIAA J., 31:49–56, 1993.

[20] D.L. Youngs. Three-dimensional numerical simulation of turbulent mixing by Rayleigh-Taylor instability. Phys. Fluids A, 3(5):1312–1320, 1991.

[21] D.L. Youngs. ILES of Rayleigh-Taylor and Richtmyer-Meshkov mixing. In ECCOMAS 2006, 2006.

[22] S. Zhang and J. T. Turner. private communication. Manchester University, UK.

Paper No. 41

Discusser's Name: Dietrich Hummel

Question:
What was the geometry for the cropped delta wing in terms of leading edge sweep, leading edge shape and AoA for vortex breakdown? Where was the flow laminar and where turbulent?

Authors' Reply: ……

Discusser's Name: J. Kamm

Question: Have you compared your Richtmyer-Meshkov results with the experimental data of J. Jacobs or K. Prestridge?

Authors' Reply: ……

Discusser's Name: Luis Eça

Question: The title of the paper includes "Computational Uncertainty in CFD". My question is how do you quantity uncertainty in ILES? What type of flow features (mean values, …) are used to quantify the uncertainty?

Authors' Reply: ……